

Amphiphilic Silane Modified Multifunctional Nanoparticles for Magnetically Targeted Photodynamic Therapy

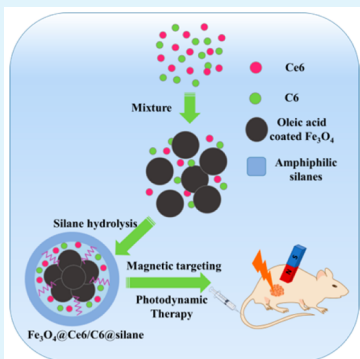
Xueke Sun, Biao Dong,* Hongwei Xu, Shihan Xu, Xinran Zhang, Yanxia Lin, Lin Xu,^{ID} Xue Bai, Shuang Zhang, and Hongwei Song^{*ID}

State Key Laboratory on Integrated Optoelectronics, College of Electronic Science and Engineering, Jilin University, 2699 Qianjin Street, Changchun 130012, P. R. China

Supporting Information

ABSTRACT: Efficient targeting is a major challenge in practical photodynamic therapy (PDT). Though the “enhanced permeability and retention” (EPR) effect is a widely used tumor targeting method, magnetic targeting strategy is more promising considering the issue of high targeting efficiency and reducing concentration-dependent toxicity. Herein, magnetic targeting and highly effective $\text{Fe}_3\text{O}_4@\text{Ce6/C6@silane}$ NPs are reported as a class of precisely controlled photosensitizers (PS) for PDT. On the basis of the amphiphilic silane encapsulation, PS chlorin e6 (Ce6) and Coumarin 6 (C6) as well as Fe_3O_4 NPs were coloaded into the inside hydrophobic environment of amphiphilic silane, forming a theranostic agent for dual-mode imaging guided and magnetic targeting enhanced *in vivo* PDT agent. To solve the problem of over-irradiation, the coloaded design of C6 and Ce6 molecules can afford the real time PDT monitoring by ratio emissions with same excitation wavelength. When $\text{Fe}_3\text{O}_4@\text{Ce6/C6@silane}$ and Ce6/C6@silane NPs are compared in *in vitro* and *in vivo* experiments, the introduction of Fe_3O_4 in the composite does not affect the PDT efficiency, whereas, in contrast, it brings MRI imaging and magnetic targeting functions. $\text{Fe}_3\text{O}_4@\text{Ce6/C6@silane}$ injection followed with magnetic field (MF) and light irradiation is important in generating an effective PDT process, showing great potential in tumor therapy.

KEYWORDS: photodynamic therapy, iron oxide, magnetic resonance imaging, amphiphilic silane, magnetic targeting



1. INTRODUCTION

Photodynamic therapy (PDT) has attracted tremendous attention for treatment of many diseases including cancers owing to its noninvasive feature and high selectivity.¹ This method involves local or systemic administration of a photosensitizer (PS), followed by irradiation of the target lesion with light of a specific wavelength, which triggers oxidative photodamage by the generation of reactive oxygen species (ROS), subsequently leading to direct tumor cell kill or damage.^{2,3} Compared with chemotherapy and radiotherapy, PDT causes minimal toxicity to normal tissues or organs due to its main advantage of rather good specificity for treatment of particular lesions that exposed to the light with certain wavelengths, and no activation of photosensitizers where in dark.^{4,5}

However, until now, there has still been some difficulties that need to be improved in PDT, such as specific targeting, biological compatibility,⁶ real time PDT feedback, etc. In recent years, delivery of nanomaterials carrying PS agents to the cancer site has been recognized on the basis of the “enhanced permeability and retention” (EPR) effect of tumors,⁷ which, however, is a passive delivery method with low efficiency, because of the pathophysiological heterogeneity among different tumors. Modifying targeting molecules on PS carriers is an important approach to enhance the tumor selectivity,⁸ which is extensively explored in PDT. However, this method also meets

the limitations of interpatient variation in receptor expressions. Magnetic field (MF) navigation can also serve as a tumor-targeting strategy that employed an external MF to attract therapeutics circulating in the bloodstream, leading to enhanced enrichment of PS carriers in tumor region.⁹ Iron oxide nanoparticles (IONPs) are always involved in the MF navigation method and explored as multifunctional composites, besides their carrier property.^{10,11} In 2011, Cui's group first combined photosensitizer Chlorin e6 with magnetic NPs to enhance the drug delivery to the cancer site.¹² Then Liu et al. developed multifunctional IONC-PEG-Ce6 NPs in 2013,⁸ which obtained MF-enhanced *in vivo* photodynamic cancer treatment. In tumor therapy, this method holds several advantages,¹³ such as the great enhancement in delivery efficiency with magnetic-targeting guidance relative to the EPR effect, and very wide applications among the tumors even with genetic variations, compared to the specific molecule based targeting way. Besides magnetic targeting design, the PDT carriers were always designed as multifunctional composites,¹⁴ which attract more and more attention. Considering the visible wavelength cannot penetrate the tissue effectively, upconversion NPs (UCNP) were employed to

Received: January 13, 2017

Accepted: February 24, 2017

Published: February 24, 2017

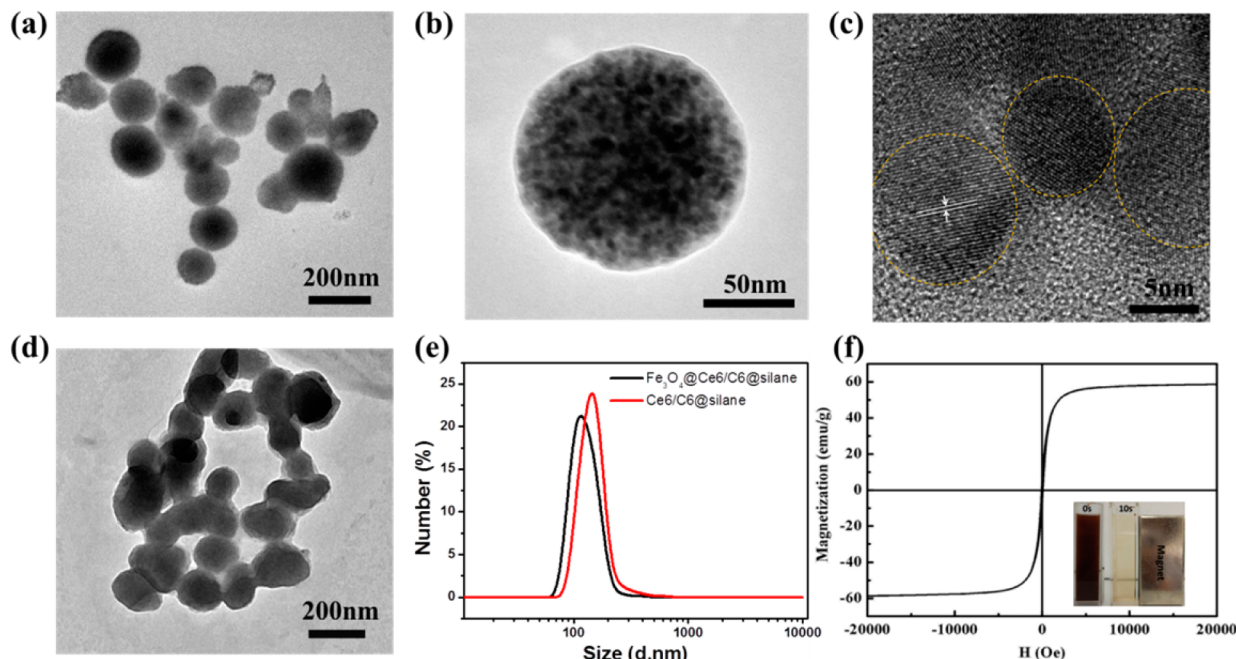


Figure 1. TEM images of (a) Fe_3O_4 @Ce6/C6@silane NPs and (b) one single Fe_3O_4 @Ce6/C6@silane NP. (c) HR-TEM image of the local area of one single Fe_3O_4 NP. (d) TEM image of Ce6/C6@silane NPs. (e) Dynamic light scattering (DLS) size distributions of Fe_3O_4 @Ce6/C6@silane (122.4 nm) and Ce6/C6@silane (142 nm). (f) Magnetization hysteresis loops of Fe_3O_4 @Ce6/C6@silane. Inset: photos of the Fe_3O_4 -containing colloidal sample that were quickly separated from a colloidal suspension by setting a magnet behind.

overcome this limitation by Liu et al.^{15–18} Besides, the multifunctional composites with a series of multimodal imaging combined PDT were developed.^{14,19,20} Shi and Bu's group integrated PDT therapy with other therapy methods for significant efficacy, such as RT (radiotherapy)/PTT (photothermal therapy) and PDT/RT treatments.^{21–23} Lin et al. designed a composite with photodynamic/photothermal/chemotherapy functions, which could also contain dual modal imaging, demonstrating the feasible application of imaging guided therapy.²⁴

In this work, to address the unresolved questions of biocompatibility, precisely PDT controlling, we developed a novel PS carrier based on the amphiphilic silane modification method we recently developed for a multifunctional platform,²⁵ which can encapsulate the hydrophobic functional molecules by hydrophobic interaction, while the outside hydrophilic hydroxyl can facilitate the bioapplications. The promising photosensitizer Chlorin e6 (Ce6) and Dye Coumarin 6 (C6) hydrophobic organic molecules were encapsulated together inside the hydrophobic environment of silane via the hydrolysis reaction, resulting in simultaneous PDT and imaging functions with the same excitation wavelengths, as shown in Figure 1. An advantage in this design is the PDT monitoring function. Note that the C6 molecule is not sensitive to red light but can be coexcited with Ce6 by 405 nm wavelength. Therefore, the ratio metric fluorescence of Ce6/C6 can be used for real-time monitoring of the consumption and then the PDT function of Ce6, which has been rarely mentioned to date. To compare the MF navigation function and EPR effect in PDT tumor treatment, IONPs (Fe_3O_4) with ultrasmall sizes were also employed as the core together with Ce6 and C6 molecules, and the composite can be called Ce6/C6@silane and Fe_3O_4 @Ce6/C6@silane, respectively. The PDT and multi-imaging (luminescent and MRI) of silane modified composites with and

without IONPs were further investigated at both cellular and animal levels.

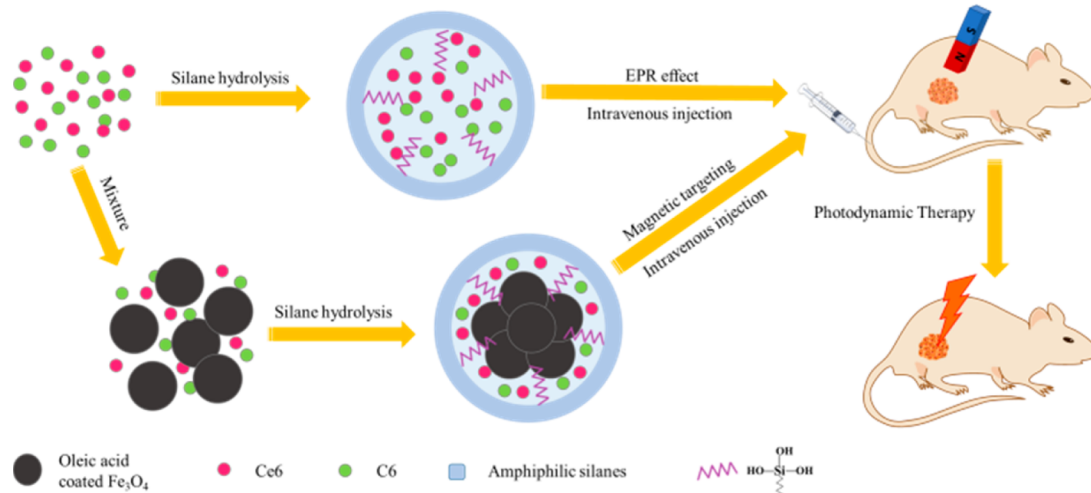
2. MATERIALS AND METHODS

2.1. Synthesis of Magnetic OA– Fe_3O_4 NPs. The Fe_3O_4 nanoparticles were prepared via the coprecipitation method. First, $\text{FeCl}_3 \cdot 6\text{H}_2\text{O}$ (5.38 g) was dissolved with deionized water (200 mL) in three-necked flask for 10 min under a flow of nitrogen. Then $\text{FeCl}_2 \cdot 4\text{H}_2\text{O}$ (1.98 g) was added into the solution, and the color of the solution changed to orange immediately. After 10 min, ammonium hydroxide solution (25%, 7 mL) was injected into the three-necked flask with vigorous stirring, and the color of the mixture changed to black immediately. The solution was stirred for an additional 3 h at room temperature and then washed with deionized water three times. The black product was dissolved in 200 mL of deionized water with oleic acid (OA, 1.22 g) dropwise added. The mixture was heated to 80 °C for 30 min with stirring under a flow of nitrogen. The OA– Fe_3O_4 NPs were dissolved in hexane for further experiments.

2.2. Synthesis of Silane-Modified OA– Fe_3O_4 NPs with Loading C6 and Ce6. The OA– Fe_3O_4 NPs (5 mg/mL, 200 μL), trimethoxy(octadecyl)silane (7.5 mg/mL, 600 μL), Chlorin e6 (Ce6, 3 mg/mL, 300 μL), and Coumarin 6 (C6, 1 mg/mL, 20 μL) were mixed in tetrahydrofuran (THF) under sonication. After 30 min, the mixture was rapidly injected to 5.5 mL water (pH ≈ 9, adjusted by addition of ammonium hydroxide) in a conical flask for the hydrolysis process under sonication. Then the conical flask was put on the bed stand at room temperature for 3–4 h, and the sample was dialyzed for 24 h at room temperature.

2.3. Singlet Oxygen Detection. To confirm the *in vitro* ${}^1\text{O}_2$ generation capability of Fe_3O_4 @Ce6/C6@silane and Ce6/C6@silane, a single oxygen probe 2,2'-bis(anthracene-9,10-diylibis(methylene))-dimalonic acid (ABDA) was used as a ${}^1\text{O}_2$ trapping reagent to quench its intrinsic absorbance after 630 nm laser irradiation at 260 nm. Solutions containing ABDA (10 ppm) and nanoparticles with different concentrations of Ce6 were exposed to 630 nm irradiation. The decrease of the absorbance caused by photobleaching of ABDA indicated ${}^1\text{O}_2$ generation.

Scheme 1. Synthesis Procedures of Ce6/C6@silane and $\text{Fe}_3\text{O}_4@\text{Ce6/C6@silane}$ NPs and the Concept of *in Vivo* Magnetically Targeted PDT^a



^aThe magnetic field around the tumor region induces local tumor accumulation of NPs.

2.4. Cell Culture. The MCF-7 cells were cultured in culture medium RPMI 1640 (Hyclone) supplemented with 10% fetal bovine serum (FBS, Clark) and 1% penicillin–streptomycin (100 U/mL penicillin and 100 g/mL streptomycin), in an incubator with 5% CO_2 and 100% humidity at 37 °C. Cells in the exponential phase of growth were used in all the experiments.

2.5. Cytotoxicity Assay. For the *in vitro* cytotoxicity test, MCF-7 cells were cultured in RPMI-1640 medium containing 10% fetal bovine serum (FBS) and 1% penicillin/streptomycin under 37 °C within 5% CO_2 atmosphere. 3-(4,5-Dimethylthiazol-2-yl)-2,15-diphenyltetrazolium bromide (MTT) assay was used to determine the cytotoxicity at various mass concentrations of samples. MCF-7 cells were seeded in 96-well plates at 1×10^4 per well and cultured for 24 h. Then $\text{Fe}_3\text{O}_4@\text{Ce6/C6@silane}$ and Ce6/C6@silane at various Ce6 concentrations were added to cells for another 24 h. After adding 10 μL of 5 mg/mL MTT solution for a further 4 h incubation (37 °C), the medium was carefully removed, and 150 μL of dimethyl sulfoxide was added. After 10–20 min dissolution, the absorbance at 490 nm was recorded using a microplate reader (Bio-Tek ELX800, USA).

2.6. *C. elegans* Culture and Imaging. The Bristol N₂ (wild type) were grown on NGM agar plates at 20 °C and fed with *E. coli* strain OP50 according to standard protocol. Approximately 15–20 young adults or L4 stage of growing hermaphrodites were picked onto NGM plates seeded with *E. coli*. For imaging, the L4 stage worms were picked onto the NGM plates seeded with *E. coli*, and an aliquot (50 μL) of $\text{Fe}_3\text{O}_4@\text{Ce6/C6@silane}$ solution (1 mg/mL) was dropped on the plate. The worms were incubated with the $\text{Fe}_3\text{O}_4@\text{Ce6/C6@silane}$ for 8 h at 20 °C, after that they were recovered onto a new bacteria seeded NGM plates for another 8 h.

2.7. *In Vivo* Fluorescence Image and MR Imaging. 4T1 tumor-bearing mice were back subcutaneous injected with Ce6/C6@silane and $\text{Fe}_3\text{O}_4@\text{Ce6/C6@silane}$ (30 mg/kg) prior to imaging. After 8 h magnetic targeting, the mice were anesthetized by intraperitoneal injection of 1% pentobarbital sodium. MR imaging was performed under a 1.2-T animal MRI scanner (HT-MRSI50-50KY) equipped with a special coil for small animals. Fluorescence imaging was performed by a small animal imaging system (Coldsping Science Corporation).

2.8. *In Vivo* Tumor Model. The Balb/c mice (female, 18–20 g body weight) were housed at room temperature with a 12 h light/dark cycle and allowed free access to food and water. All the mice were used under protocols approved by the laboratory animal center of Jilin University. After about 2 weeks observation, Balb/c mice were subcutaneously injected at the right hind leg with 0.1 mL of 4T1 cells (1×10^7 cells/mL). When the tumor reached a size of 80–100 mm³,

the tumor-bearing mice were randomly assigned to different groups as follows: (1) control; (2) $\text{Ce6/C6@silane+light}$; (3) $\text{Fe}_3\text{O}_4@\text{Ce6/C6@silane+light}$; (4) $\text{Fe}_3\text{O}_4@\text{Ce6/C6@silane+light+magnetic targeting}$. Tumors from control, Ce6/C6@silane , and $\text{Fe}_3\text{O}_4@\text{Ce6/C6@silane}$ injected mice with or without magnetic tumor targeting were exposed to the 630 nm light at 5 mW·cm⁻² for 40 min. All animal experiments were carried out with the approval of the university's institutional animal care and use committee. The tumor size was monitored by a vernier caliper and the tumor volume (V) was calculated as $V = L \times W^2 / 2$, where L and W were the length and width of the tumor, respectively.

2.9. Histological Examination by H&E Staining. Tumor tissues and the main organs of different groups were fixed with 4% paraformaldehyde solution. Samples were then paraffin-embedded, sectioned, and stained with hematoxylin and eosin (H&E). Histopathological changes were observed under a light microscope.

3. RESULTS AND DISCUSSION

3.1. Synthesis and Characterization of Multifunctional Nanoparticles. The schematic illustrations in Scheme 1 show the preparation of Ce6/C6@silane and $\text{Fe}_3\text{O}_4 @\text{Ce6/C6@silane}$. Chlorin e6(Ce6) is a famous PS, which can generate singlet oxygen with the irradiation at 630 nm. The reason for choosing C6 as the coloading molecule is that both molecules can be coexcited under 405 nm wavelength and the luminescent intensity of C6 would not change under the irradiation at 630 nm. In brief, Ce6 and C6 hydrophobic organic molecules were loaded into the inside hydrophobic space of silane via the hydrolysis reaction. Following the same method, Fe_3O_4 NPs with a size of 8 nm (Figure S1) can also loaded into the silane coating composites without changing any experimental factors. The amphiphilic silane plays the carrier function and also greatly improves the biocompatibility. Compared to other surface modification methods, this protocol is more simple and versatile without high temperature reaction.²⁴ Magnetic Fe_3O_4 NPs could also be visualized by magnetic resonance imaging (MRI), which has been widely applied in a variety of clinical diagnostic fields as a powerful noninvasive technique.²⁶ A series of *in vitro* and *in vivo* experiments are designed to carefully evaluate the stability and PDT efficiency of Ce6/C6@silane and $\text{Fe}_3\text{O}_4@\text{Ce6/C6@silane}$, containing cellular uptake, light-induced cell killing,

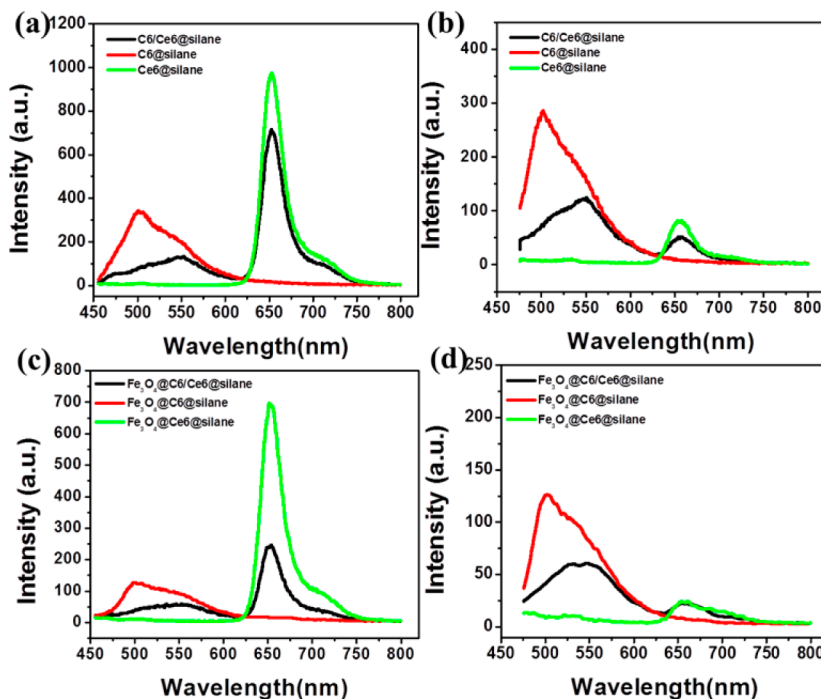


Figure 2. Fluorescence emission spectra of Ce6/C6@silane, C6@silane, and Ce6@silane with excitation at (a) $\lambda_{\text{ex}} = 405 \text{ nm}$ and (b) $\lambda_{\text{ex}} = 450 \text{ nm}$. Fluorescence emission spectra of Fe₃O₄@Ce6/C6@silane, Fe₃O₄@C6@silane, and Fe₃O₄@Ce6@silane with excitation at (c) $\lambda_{\text{ex}} = 405 \text{ nm}$ and (d) $\lambda_{\text{ex}} = 450 \text{ nm}$.

circulation *in vivo*, optical imaging and MRI, as well as under magnetic tumor targeting and MF-enhanced PDT of Fe₃O₄@Ce6/C6@silane NPs at both cellular and animal levels.

The TEM image of Fe₃O₄@Ce6/C6@silane in Figure 1a shows basically spherical morphology after silane encapsulation with a size of 120–150 nm. The HR-TEM image of a single Fe₃O₄@Ce6/C6@silane particle in Figure 1b indicates that an aggregation of Fe₃O₄ NPs happened in the hydrolysis process, which can be further confirmed by the enlarged HR-TEM image on the local area of a single composite particle in Figure 1c. Clear lattice fringes with the 0.253 nm lattice is in accordance with (311) planes of Fe₃O₄ NPs. The TEM image of Ce6/C6@silane composites was shown in Figure 1d, and the size can be determined by DLS measurement, as shown in Figure 1e. The DLS results show that the mean size of Fe₃O₄@Ce6/C6@silane (122.4 nm) is smaller than that of Ce6/C6@silane (142 nm), and both composites have relatively narrow size distributions and most NPs are safely below 150 nm. Note that the ζ potential of both Fe₃O₄@Ce6/C6@silane and Ce6/C6@silane are below −30 (Figure S3), indicating high water dispersity and solubility. A magnetization hysteresis loop of Fe₃O₄@Ce6/C6@silane was shown in Figure 1f. The inset digital pictures of a Fe₃O₄-containing colloidal sample intuitively showed the magnetic nature of Fe₃O₄ NPs, which were quickly separated from a colloidal suspension with the dark color fading remarkably by setting a magnet behind. The TEM image and XRD pattern of Fe₃O₄ were shown in Figure S1 and Figure S2, respectively.

Panels a and b of Figure 2 show the emission spectra of Ce6/C6@silane, Ce6@silane, and C6@silane NPs under excitation of 405 and 450 nm, respectively. The green emission band centered at 510 nm and the red emission at 650 nm belong to C6 and Ce6 molecules, respectively, which can be coexcited by both wavelength of 405 and 450 nm. The favorable excitation wavelength of Ce6 is 405 nm, and that of C6 is 450 nm. There

is an obvious shape change in the C6 emission spectra between Ce6@silane and Ce6/C6@silane, which may be attributed to the energy transfer from C6 to Ce6,²⁷ even though no enhanced emission intensity of Ce6 is observed. Panels c and d of Figure 2 show the emission spectra of Fe₃O₄@Ce6/C6@silane, Fe₃O₄@C6@silane, and Fe₃O₄@Ce6@silane NPs under excitation of 405 and 450 nm, respectively. The Fe₃O₄-containing samples show the same trend in emission spectra as the samples without IONPs. From the luminescent spectra of Ce6, besides the PDT function, it can also serve as imaging agent. In fact, the red emission intensity is consistent with the PDT consumption of Ce6 molecules and can be utilized as simultaneously monitoring probe during the PDT, which is further discussed in the following cellular experimental part. UV-vis absorption spectra and fluorescence excitation spectra of Ce6/C6@silane and Fe₃O₄@Ce6/C6@silane were shown in Figure S4.

3.2. Singlet Oxygen ${}^1\text{O}_2$ Detection and Cytotoxicity Assessment.

To study the PDT property of Ce6/C6@silane and Fe₃O₄@Ce6/C6@silane NPs with different amount of Ce6 molecules (from 0.05 $\mu\text{g}/\text{mL}$ Ce6 to 0.15 $\mu\text{g}/\text{mL}$ Ce6), the singlet oxygen (${}^1\text{O}_2$) induced by Ce6 under irradiation was evaluated with 2,2'-bis(anthracene-9,10-diylbis(methylene))-dimalonic acid (ABDA) as an ${}^1\text{O}_2$ indicator.²⁸ As illustrated in Figure 3a, under the red light irradiation (620–630 nm, 5 $\text{mW}\cdot\text{cm}^{-2}$) on the solution, the absorption of the ABDA decreases significantly at a wavelength of 260 nm. The decay of ABDA absorption (260 nm) is positive correlation with the consumption of Ce6 and the generation of ${}^1\text{O}_2$, the higher Ce6 concentration, and the higher singlet oxygen generation efficiency. In this case, 0.15 $\mu\text{g}/\text{mL}$ Ce6 is the highest concentration in preparation because higher concentration will cause the instability.

Further, the PDT measurement with Ce6/C6@silane samples corresponding to Figure 3a,c on MCF-7 cells were

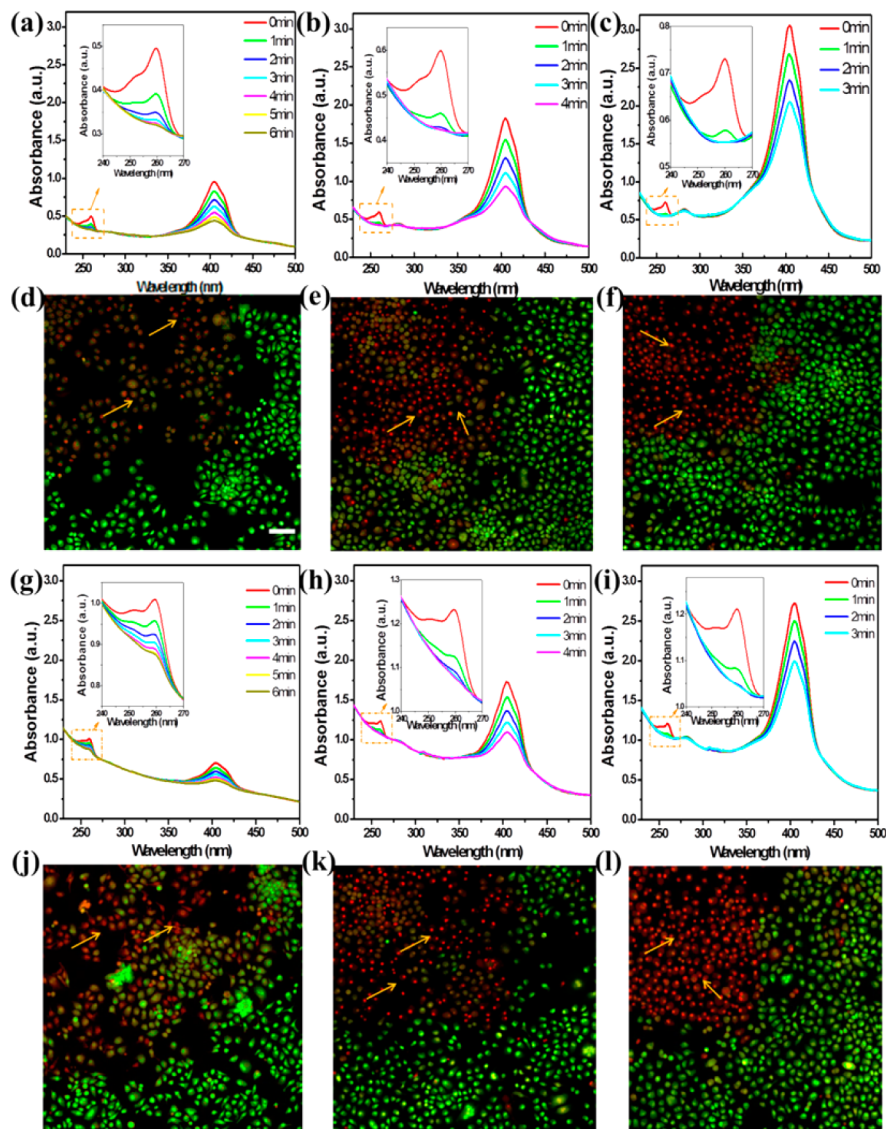


Figure 3. UV-vis absorption spectra of singlet oxygen probe (ABDA) mixed with 15.6 µg/mL Ce6/C6@silane with different amounts of Ce6: (a) 0.05 µg/mL Ce6; (b) 0.1 µg/mL Ce6; (c) 0.15 µg/mL Ce6. The spectra were measured every 1 min after red light irradiation (630 nm, 5 mW·cm⁻²). (d)–(f) Confocal microscopic images of MCF-7 cells treated by the corresponding Ce6/C6@silane NPs (1.2 µg/mL) with different amounts of Ce6 for 4 h after local irradiation by the 635 nm laser for 20 s. The cells were stained with AO (green) and EB (red). (g)–(i) UV-vis absorption changes of ABDA mixed with 12 µg/mL Fe₃O₄@Ce6/C6@silane NPs with different amounts of Ce6 [(g) 0.05 µg/mL Ce6; (h) 0.1 µg/mL Ce6; (i) 0.15 µg/mL Ce6] and different exposure times (630 nm, 5 mW·cm⁻²). (j)–(l) Confocal microscopic images of MCF-7 cells treated by the above corresponding Fe₃O₄@Ce6/C6@silane NPs (1 µg/mL) for 4 h and then stained with AO (green) and EB (red) after local irradiation by the 635 nm laser for 20 s. The scale bar is 100 µm.

performed by using confocal laser scanning microscopy (CLSM, Olympus FV1000). Briefly, MCF-7 cells were incubated with Ce6/C6@silane NPs with different Ce6 concentrations (from 0.05 µg/mL Ce6 to 0.15 µg/mL Ce6) for 4 h. Panels a and d of Figure 3 show the results after irradiation with a 635 nm laser for 20 s by CLSM. The therapeutic effect of Ce6/C6@silane samples was measured in the presence of AO&EB dye, which is a widely accepted apoptosis assay. Here, we can easily observe the clear boundary of the green region emitted by AO (alive cells) and red region emitted by EB (apoptotic cells), indicating the highly PDT efficiency of the composites. The yellow arrow marks illustrate the cells under apoptosis assay, and there are only several apoptotic cells in the irradiation spot in Figure 3d, while most of the cells in the area are apoptosis after the same irradiation

time in Figure 3f. Therefore, on the basis of the contribution of green and red color in the irradiation spot, it is clear that Ce6/C6@silane with a high concentration of Ce6 shows a better therapeutic effect of PDT compared with that of Ce6/C6@silane with a low concentration of Ce6.

Panels g and i of Figure 3 show the decay of ABDA absorption (260 nm) with the sample of Fe₃O₄@Ce6/C6@silane with different Ce6 concentrations. In addition, the same cellular experiments were also performed with the Fe₃O₄-containing samples, as shown in Figure 3j,l. Though the Fe₃O₄ were loaded inside the Ce6/C6@silane NPs, no influence was found on the PDT ability and the trend of consumption of Ce6 and the generation of ¹O₂ is similar to that of Ce6/C6@silane NPs.

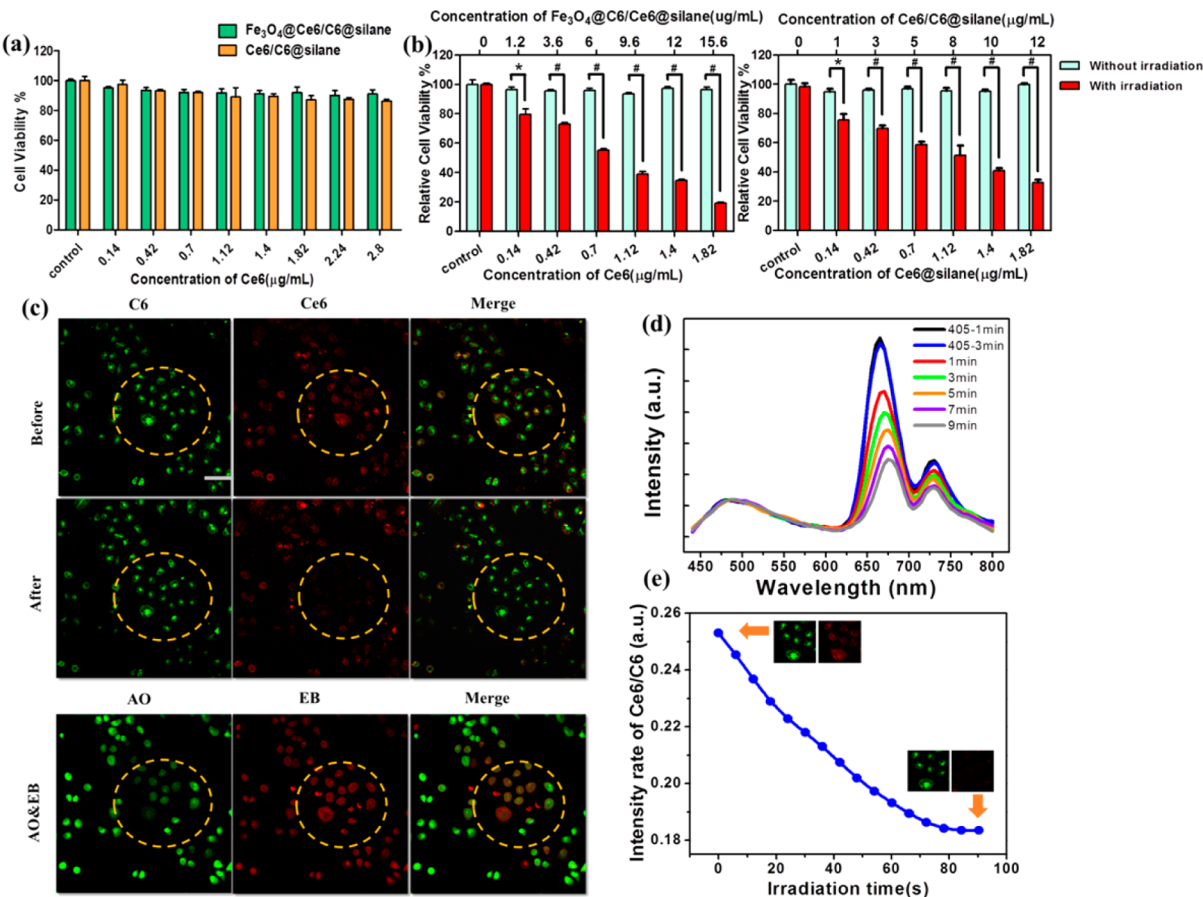


Figure 4. (a) Cell viability of MCF-7 cells after incubation with $\text{Fe}_3\text{O}_4@\text{Ce6/C6@silane}$ or Ce6/C6@silane NPs with same Ce6 concentration of $0.15 \mu\text{g}/\text{mL}$ for 24 h without irradiation in the dark. (b) Phototoxicity of $\text{Fe}_3\text{O}_4@\text{Ce6/C6@silane}$ and Ce6/C6@silane with $0.15 \mu\text{g}/\text{mL}$ Ce6 to MCF-7 cells under red light irradiation (630 nm , $5 \text{ mW}\cdot\text{cm}^{-2}$, 30 s). (c) Confocal microscopy images of MCF-7 cells incubated with $\text{Fe}_3\text{O}_4@\text{Ce6/C6@silane}$ containing $0.15 \mu\text{g}/\text{mL}$ Ce6 before and after 635 nm irradiation ($\lambda_{\text{ex}} = 405 \text{ nm}$). Then the cells were stained with AO&EB dye for 15 min ($\lambda_{\text{ex}} = 488 \text{ nm}$). The scale bar is $100 \mu\text{m}$. (d) Under 405 nm excitation, the ratio metric emission spectra of $\text{Fe}_3\text{O}_4@\text{Ce6/C6@silane}$ were recorded once every 2 min after irradiation with 405 and 630 nm ($5 \text{ mW}\cdot\text{cm}^{-2}$). (e) Ratio metric intensity of Ce6/C6 based on the grayscale value of the confocal images from different detection channels in the irradiation time 0–90 s. Inset: the first two and last two images for illustration of the Ce6 consumption. P values: *, $P < 0.05$; #, $P < 0.01$.

3.3. Toxicity Assessment and PDT Effect in MCF-7 Cells. A successful PDT photosensitizer needs to exhibit low cytotoxicity in the dark but significant cancer cell death when exposed to light. In our *in vitro* study, the cytotoxicity of $\text{Fe}_3\text{O}_4@\text{Ce6/C6@silane}$ and Ce6/C6@silane to MCF-7 cells was examined by using the MTT assay, both in the presence and the absence of irradiation with 630 nm light (Figure 4a). Because Ce6 molecules play the major PDT function, we tested the dark cytotoxicity of $\text{Fe}_3\text{O}_4@\text{Ce6/C6@silane}$ and Ce6/C6@silane NPs on the basis of the same Ce6 weight concentration with the range 0.14 – $2.24 \mu\text{g}/\text{mL}$. $\text{Fe}_3\text{O}_4@\text{Ce6/C6@silane}$ and Ce6/C6@silane NPs exhibit negligible dark toxicity to MCF-7 cell viability. Even treated with the highest dosage $2.8 \mu\text{g}/\text{mL}$ Ce6, the MCF-7 cell viability of that treated with $\text{Fe}_3\text{O}_4@\text{Ce6/C6@silane}$ is over 90% and with Ce6/C6@silane is over 85%. Note that $\text{Fe}_3\text{O}_4@\text{Ce6/C6@silane}$ NPs show better dark cytotoxicity than Ce6/C6@silane due to the stability. These results indicate the good biocompatibility of two kinds of NPs on MCF-7 cells, especially within the Ce6 concentration 0.14 – $1.82 \mu\text{g}/\text{mL}$.

Figure 4b shows the PDT effect of $\text{Fe}_3\text{O}_4@\text{Ce6/C6@silane}$ and Ce6/C6@silane on MCF-7 cells under 630 nm light irradiation ($5 \text{ mW}\cdot\text{cm}^{-2}$, 30 s) detected by MTT assay. The cell

viability was normalized to control cells (with drug but no irradiated). Under the light exposure, in contrast to the dark cytotoxic experiments, $\text{Fe}_3\text{O}_4@\text{Ce6/C6@silane}$ and Ce6/C6@silane NPs showed remarkable and concentration dependent phototoxicity. The increased proportions of cell death in the Ce6-containing NPs treated cells could be attributed to the increased cellular uptake, and subsequently more ROS production. As the concentration of $\text{Fe}_3\text{O}_4@\text{Ce6/C6@silane}$ was $15.6 \mu\text{g}/\text{mL}$ (Ce6: $1.82 \mu\text{g}/\text{mL}$), over 80% of the cells were dead. With same Ce6 concentration ($1.82 \mu\text{g}/\text{mL}$), Ce6/C6@silane NPs caused 70% loss of cell viability. Both groups treated with the drug, while without light exposure, showed no cytotoxic effects in the concentration range 0.14 – $1.82 \mu\text{g}/\text{mL}$ Ce6 on tumor cells, which is consistent with the result of cytotoxicity assessment in the dark. The two kinds of NPs show excellent biocompatibility as well as good photocytotoxicity upon irradiation, suggesting the great potential as a powerful agent for PDT treatment.

Besides the PDT effect with red irradiation, Ce6 molecules also emit red light with 405 nm excitation, as discussed above, which can serve as a fluorescence imaging agent, though rarely explored before. In addition, we found that the red emission from Ce6 is positively correlated with the consumption of Ce6

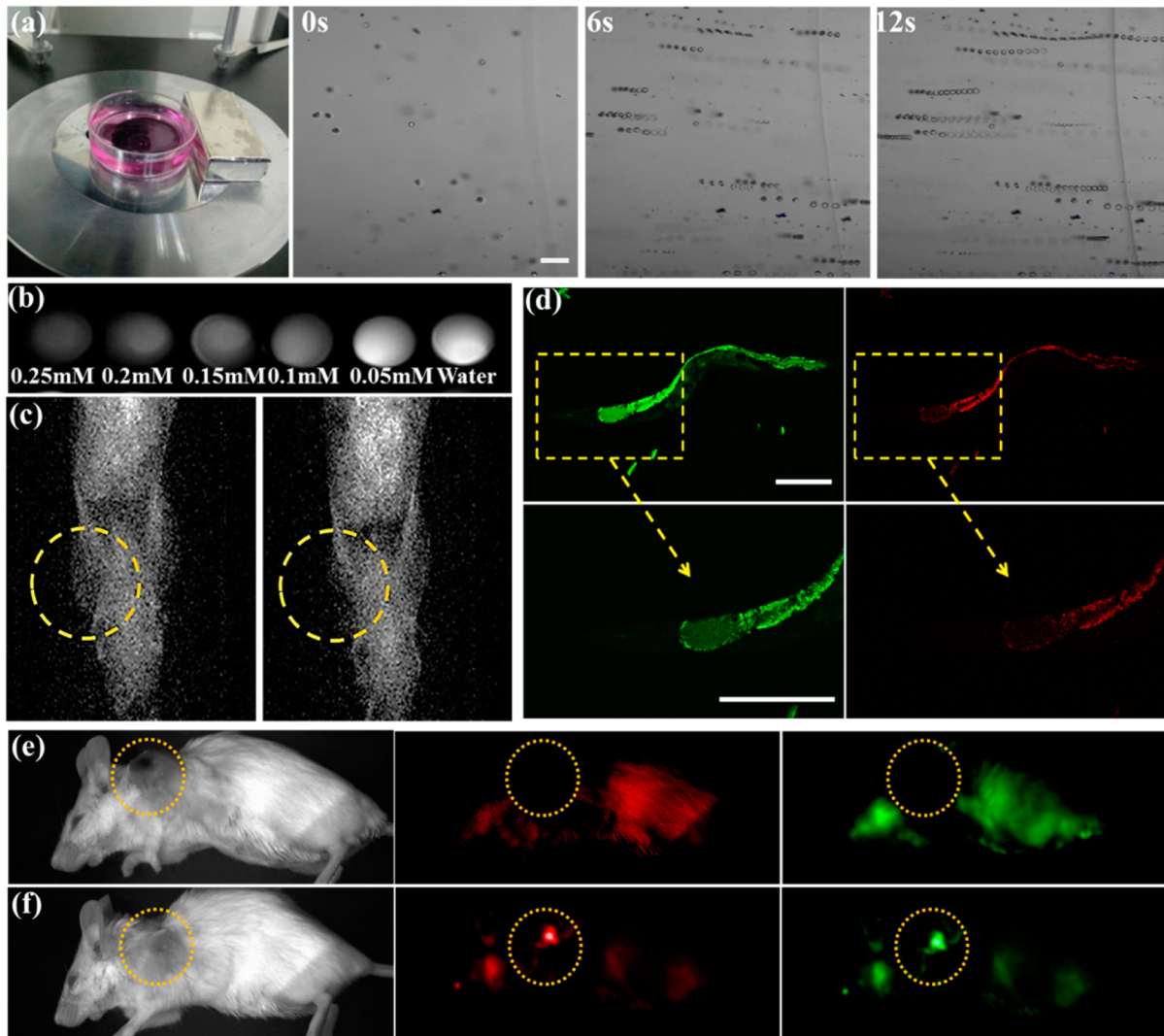


Figure 5. (a) MCF-7 cells intubated with Fe₃O₄@Ce6/C6@silane and then attracted to the lip of a Petri dish when the magnet was setting. The scale bar is 100 μ m. (b) T₂-MRI of Fe₃O₄@Ce6/C6@silane in aqueous solution with different Fe₃O₄ concentrations (T₂ relaxation time: 5.28 ms, 7.70 ms, 9.12 ms, 12.13 ms, 24.35 ms, 176.24 ms). (c) T₂-weighted MR images before (left) and after (right) back subcutaneous injection with Fe₃O₄@Ce6/C6@silane followed with the 8h magnetic field targeting. (d) Confocal microscopy images of *N₂ Caenorhabditis elegans* (λ_{ex} = 405 nm), C6 (green signal), and Ce6 (red signal). The scale bar is 200 μ m. *In vivo* fluorescence image of 4T1 tumor-bearing mice. 4T1 tumor-bearing mice were back subcutaneous injected with Fe₃O₄@Ce6/C6@silane before (e) and after 8 h of magnetic accumulation on the tumor site (f).

and generation of singlet oxygen, which means the PDT situation can be monitored by the emission intensity. In Figure 4c, we incubated the MCF-7 cells with Fe₃O₄@Ce6/C6@silane NPs for 4 h and then gave the cells a local irradiation at 635 nm for 20 s.

By comparing the spot before and after irradiation, it can be observed that the red signal of Ce6 in the circle area is difficult to detect due to the consumption of Ce6, while the emission from C6 (green signal) keeps the intensity. To further conform, apoptosis assay AO&EB dye were utilized and the red color in the irradiation area indicated the efficient PDT treatment. Afterward, MCF-7 cells treated with Fe₃O₄@Ce6/C6@silane were monitored by fluorescence imaging in Figure S5. The outer membrane of MCF-7 cells is ruptured. We can see that an intense homogeneous green signal (C6) is around the nucleolus, and in the same time Ce6 is consumed, indicating that the red signal is difficult to detect.

It is very important to precisely monitor and control the PDT at the cellular or animal level to avoid extra injury from

over-irradiation. In this composite structure, the ratio emission of C6 and Ce6 can be employed for precise monitoring because the luminescent intensity of C6 would not change after the irradiation at 405 or 635 nm. As shown in Figure 4d, in first 3 min, both the emission spectra of C6 and Ce6 do not change under the continuous irradiation of 405 nm wavelength. After 635 nm wavelength irradiation for an increased time, the red emission of Ce6 continues to decrease. Therefore, for a certain Fe₃O₄@Ce6/C6@silane sample, the ratio of red/green emission can be used as a PDT probe in the therapy process. We also tested the ratio of the luminescent intensity of C6 and Ce6 for 90 s with the irradiation at 635 nm in the PDT process of MCF-7 cells. The ratio of the gray value strength of the Ce6 and C6 images decreases as the irradiation time increases to 90 s. The first two images and last two images were given as insets, clearly illustrating the consumption of Ce6. Note that the ratio of the Ce6 and C6 molecules changes much faster than that calculated with the spectra due to the much higher power density of the irradiation laser. Therefore, the imaging function

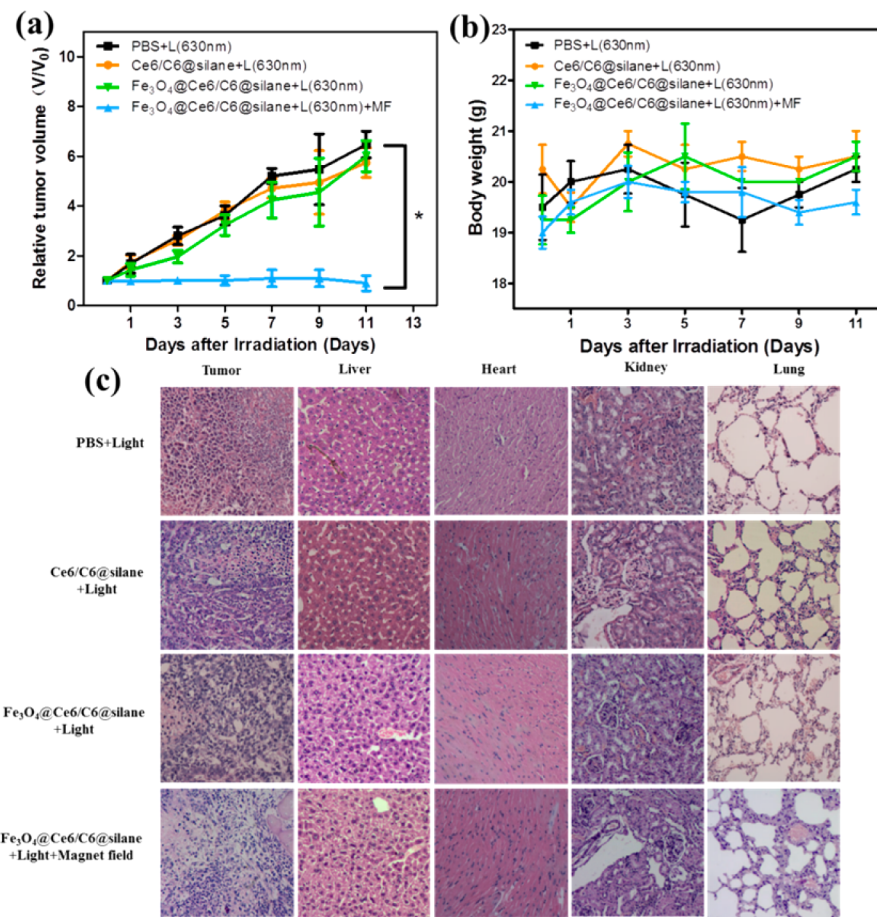


Figure 6. *In vivo* PDT treatment of 4T1 tumor-bearing mice. (a) The tumor growth curves of mice after various treatments are as indicated. The relative tumor volumes were normalized to their initial sizes. Four mice were used in each group. (b) Average body weights from different groups collected at 11 day after the treatment. (c) H&E staining of tumor and major organs slice collected from mice from various groups at 24 h post PDT treatment (630 nm, 5 mW·cm⁻² for 40 min). The scale bar is 100 μ m. *P* values: *, *P* < 0.01.

of composites not only can track the molecules but also can monitor the degree of PDT treatment.

3.4. Dual-Model Imaging *In Vivo*. An important issue of this work is to compare the EPR effect and magnetic targeting with $\text{Fe}_3\text{O}_4@\text{Ce6/C6@silane}$ and Ce6/C6@silane NPs. The cell movement by $\text{Fe}_3\text{O}_4@\text{Ce6/C6@silane}$ NPs was tested first. As shown in Figure 5a, a magnet was set near a cell culture dish with MCF-7 cells incubated with $\text{Fe}_3\text{O}_4@\text{Ce6/C6@silane}$. After that, MCF-7 cells start to move along the magnetic field direction and the movement traces could be described by pictures overlaid at 0, 6, and 12 s, indicating the efficient magnetic targeting property. Relative to Ce6/C6@silane , besides magnetic targeting, $\text{Fe}_3\text{O}_4@\text{Ce6/C6@silane}$ has another advantage in MRI imaging.

T_2 -weighted MR imaging reveals a concentration-dependent darkening effect in Figure 5b. As the Fe concentration increases, the signal intensity of the MR images increases, as expected for T_2 contrast agents. MR imaging was also employed to monitor PDT *in vivo*. MRI signals of a treated mouse were monitored by a MRI scanner (HT-MRSI50-50KY) before and after magnetic navigation targeting treatment with a magnet for 8 h, as shown in Figure 5c. As a result, the signal of local tumor (yellow circle) is enhanced due to the INOP treatment and magnetic attraction, forming a clear contrast compared with that of the same local tumor tissue before treatment, which further confirms the prominent accumulation

of $\text{Fe}_3\text{O}_4@\text{Ce6/C6@silane}$ in the tumor exposed to the magnetic field. Conversely, there are no obvious changes observed in the MR images of the tumor tissues in the control group (not shown).

As dual mode imaging NPs, the luminescent imaging property was also tested with *C. elegans* and mouse. *C. elegans* is a free living soil nematode with a simple and well-defined anatomy. Its body is optically transparent which allows *in vivo* imaging of the whole organism as well as *in situ* determination of the biodistribution of the internalized fluorescent NPs and assessment of their toxic effects at the same time.²⁹ We fed the N₂ type *C. elegans* with $\text{Fe}_3\text{O}_4@\text{Ce6/C6@silane}$ NPs for 8 h and then provided the worms a new nanoparticles-free plate for another 8 h. The $\text{Fe}_3\text{O}_4@\text{Ce6/C6@silane}$ in the intestinal lumen and rectum of *C. elegans* can clearly be seen by their green and red emission ($\lambda_{\text{ex}} = 405 \text{ nm}$), as shown in Figure 5d. No signal was found in the pharyngeal, indicating good metabolism of $\text{Fe}_3\text{O}_4@\text{Ce6/C6@silane}$. In the ventral nerve cord and gonad arm, signal can hardly be detected due to the good integrity of the $\text{Fe}_3\text{O}_4@\text{Ce6/C6@silane}$ NPs.

4T1 tumor-bearing mice were selected as the animal model. The tumors which were implanted and grown in mice to appropriate size (about 80–100 mm³) were treated with a back subcutaneous injected of $\text{Fe}_3\text{O}_4@\text{Ce6/C6@silane}$ NPs (30 mg/kg). Fluorescence imaging by C6 and Ce6 molecules was done with an *in vivo* imaging system. The tumor site of the

group with 8 h magnetic targeting could be detected with the luminescent signal from both C6 and Ce6, as shown in Figure 5f. In contrast, no luminescent signal could be detected without magnetic targeting, as shown in Figure 5e. The *in vivo* fluorescence/MR dual modal imaging tests also suggested the efficient magnetic tumor targeting effect with Fe₃O₄@Ce6/C6@silane NPs.

3.5. *In Vivo* Magnetically Targeted PDT. We next examined the *in vivo* PDT effect of Fe₃O₄@Ce6/C6@silane and Ce6/C6@silane NPs by irradiating with lamp light (630 nm, 5 mW·cm⁻² for 40 min) after 8 h post-intravenous injection (200 μL, 1.2 mg/mL). The 4T1 tumor-bearing mice were randomly divided into four groups, each group containing four mice: (1) injected with PBS and light (control); (2) injected with Ce6/C6@silane and light; (3) injected with Fe₃O₄@Ce6/C6@silane exposed to the light but without magnetic targeting; (4) injected with Fe₃O₄@Ce6/C6@silane and exposed to the laser under the magnetic field. The PDT treatment was conducted 24 h after intravenous injection and tumor sizes were measured every 2 days. No tumor growth inhibition was observed in the group of mice with red light irradiation only (group 1), which indicated that irradiation with such a low power intensity NIR had little photothermal effect. In group 2, no tumor inhibition was observed, which showed that Ce6/C6@silane and laser was not enough due to EPR effect only. Group 3 (Fe₃O₄@Ce6/C6@silane with light) also did not display an obvious therapeutic effect, which suggested that magnetic navigation was important for targeting tumor tissue.

In contrast, the tumor growths of treatment group 4 were remarkably suppressed. Tumor growth inhibition (TGI) was found to be around 86.15%, indicating Fe₃O₄@Ce6/C6@silane injection followed with magnetic field and light irradiation is important in generating an effective PDT process. Neither significant weight loss nor any abnormal behavior was observed in all groups (Figure 6b). From the H&E staining analysis, morphology change and necrosis were observed, as shown in Figure 6c. The tumor tissue also showed clear necrosis with Fe₃O₄@Ce6/C6@silane injection plus 630 nm light irradiation with magnetic field, whereas barely any damage was observed for tumors of the other three groups, which indicates that Fe₃O₄@Ce6/C6@silane can be effectively activated with a magnetic field and red light irradiation to be intensely phototoxic to the tumor. The H&E stained images of the main organs from four groups suggest that our multifunctional nanoparticles did not induce appreciable toxic side effects to treated mice.

4. CONCLUSIONS

We have developed the multifunctional Fe₃O₄@Ce6/C6@silane NPs, which are suitable candidates with fluorescence/MRI dual mode imaging and magnetic targeting and controlled PDT ability. The silane modification makes the composites stable and biocompatible. Ratio metric emissions of C6 and Ce6 can be employed here for precisely monitoring of PDT level to avoid over-irradiation. By comparison of Fe₃O₄@Ce6/C6@silane and Ce6/C6@silane NPs in *in vitro* and *in vivo* experiments, the introduction of Fe₃O₄ in the composite does not affect the PDT efficiency, whereas, in contrast, it brings MRI imaging and magnetic targeting functions. In addition, our results indicate that the EPR effect is not enough. Fe₃O₄@Ce6/C6@silane injection followed with magnetic field targeting and light irradiation is important in generating an effective PDT

process. This structural design may also pave the way for their use in treating deep-tissue cancer, especially in situations not accessible to regular cancer treatment.

■ ASSOCIATED CONTENT

● Supporting Information

The Supporting Information is available free of charge on the ACS Publications website at DOI: 10.1021/acsmami.7b00647.

TEM images and XRD patterns of Fe₃O₄, ζ potentials, UV-vis spectra, CLSM of cell morphology, photographs of sample solubility and stability (PDF)

■ AUTHOR INFORMATION

Corresponding Authors

*E-mail: dongb@jlu.edu.cn (Biao Dong).

*E-mail: songhw@jlu.edu.cn (Hongwei Song).

ORCID

Lin Xu: 0000-0001-5831-430X

Hongwei Song: 0000-0003-3897-5789

Author Contributions

Xueke Sun conducted most of the investigation for the samples and wrote the main paper. Biao Dong supervised the project, gave valuable advice on the proceeding of this work, and revised the manuscript. Hongwei Song provided precious suggestions on the selection of tests and analysis of experimental data about the preparation of the materials. Lin Xu, Xue Bai, and Shuang Zhang gave advice on the experimental scheme, Hongwei Xu, Shihuan Xu, Xinran Zhang, and Yanxia Lin supported the characterization of the samples. All authors discussed the results and commented on the manuscript at all stages.

Notes

The authors declare no competing financial interest.

■ ACKNOWLEDGMENTS

This work was supported by the National Key Research and Development Program (2016YFC0207101), Major State Basic Research Development Program of China (973 Program) (no. 2014CB643506), the program of Chang Jiang Scholars and Innovative Research Team in University (No. IRT13018), the National Natural Science Foundation of China (Grant no. 11374127, 11304118, 81301289, 21403084 and 11674127), and the Norman Bethune Program of Jilin University (2015316).

■ REFERENCES

- (1) Bonnett, R. Photosensitizers of the Porphyrin and Phthalocyanine Series for Photodynamic Therapy. *Chem. Soc. Rev.* **1995**, *24*, 19–33.
- (2) Shanmugam, V.; Selvakumar, S.; Yeh, C. S. Near-infrared Light-Responsive Nanomaterials in Cancer Therapeutics. *Chem. Soc. Rev.* **2014**, *43*, 6254–87.
- (3) Idris, N. M.; Gnanasammandhan, M. K.; Zhang, J.; Ho, P. C.; Mahendran, R.; Zhang, Y. *In Vivo* Photodynamic Therapy Using Upconversion Nanoparticles as Remote-controlled Nanotransducers. *Nat. Med.* **2012**, *18*, 1580–5.
- (4) Lin, J.; Wang, P.; Huang, P.; Wang, Z.; Chen, S.; Niu, G.; Li, W.; He, J.; Cui, D.; Lu, G.; Chen, X.; Nie, Z. Photosensitizer-Loaded Gold Vesicles with Strong Plasmonic Coupling Effect for Imaging-Guided Photothermal/Photodynamic Therapy. *ACS Nano* **2013**, *7*, 5320–5329.
- (5) Song, X.; Liang, C.; Gong, H.; Chen, Q.; Wang, C.; Liu, Z. Photosensitizer-Conjugated Albumin-Polypyrrole Nanoparticles for

- Imaging-Guided *In Vivo* Photodynamic/Photothermal Therapy. *Small* **2015**, *11*, 3932–41.
- (6) Liu, B.; Zhang, X.; Li, C.; He, F.; Chen, Y.; Huang, S.; Jin, D.; Yang, P.; Cheng, Z.; Lin, J. Magnetically Targeted Delivery of DOX Loaded Cu₉S₈@mSiO₂@Fe₃O₄-PEG Nanocomposites for Combined MR Imaging and Chemo/Photothermal Synergistic Therapy. *Nanoscale* **2016**, *8*, 12560–9.
- (7) Nichols, J. W.; Bae, Y. H. EPR: Evidence and Fallacy. *J. Controlled Release* **2014**, *190*, 451–64.
- (8) Li, Z.; Wang, C.; Cheng, L.; Gong, H.; Yin, S.; Gong, Q.; Li, Y.; Liu, Z. PEG-functionalized Iron Oxide Nanoclusters Loaded with Chlorin e6 for Targeted, NIR Light Induced, Photodynamic Therapy. *Biomaterials* **2013**, *34*, 9160–70.
- (9) Zhou, Z.; Sun, Y.; Shen, J.; Wei, J.; Yu, C.; Kong, B.; Liu, W.; Yang, H.; Yang, S.; Wang, W. Iron/Iron Oxide Core/Shell Nanoparticles for Magnetic Targeting MRI and Near-infrared Photothermal Therapy. *Biomaterials* **2014**, *35*, 7470–8.
- (10) Cheng, F. Y.; Su, C. H.; Yang, Y. S.; Yeh, C. S.; Tsai, C. Y.; Wu, C. L.; Wu, M. T.; Shieh, D. B. Characterization of Aqueous Dispersions of Fe₃O₄ Nanoparticles and Their Biomedical Applications. *Biomaterials* **2005**, *26*, 729–738.
- (11) Choi, J. W.; Park, J. W.; Na, Y.; Jung, S. J.; Hwang, J. K.; Choi, D.; Lee, K. G.; Yun, C. O. Using a Magnetic Field to Redirect an Oncolytic Adenovirus Complexed with Iron Oxide Augments Gene Therapy Efficacy. *Biomaterials* **2015**, *65*, 163–74.
- (12) Huang, P.; Li, Z.; Lin, J.; Yang, D.; Gao, G.; Xu, C.; Bao, L.; Zhang, C.; Wang, K.; Song, H.; Hu, H.; Cui, D. Photosensitizer-Conjugated Magnetic Nanoparticles for *In Vivo* Simultaneous Magnetofluorescent Imaging and Targeting Therapy. *Biomaterials* **2011**, *32*, 3447–3458.
- (13) Cheng, L.; Yang, K.; Li, Y.; Zeng, X.; Shao, M.; Lee, S. T.; Liu, Z. Multifunctional Nanoparticles for Upconversion Luminescence/MR Multimodal Imaging and Magnetically Targeted Photothermal Therapy. *Biomaterials* **2012**, *33*, 2215–22.
- (14) Dou, Q.; Idris, N. M.; Zhang, Y. Sandwich-Structured Upconversion Nanoparticles with Tunable Color for Multiplexed Cell Labeling. *Biomaterials* **2013**, *34*, 1722–31.
- (15) Kim, M. H.; Son, H. Y.; Kim, G. Y.; Park, K.; Huh, Y. M.; Haam, S. Redoxable Heteronanoocrystals Functioning Magnetic Relaxation Switch for Activatable T1 and T2 Dual-Mode Magnetic Resonance Imaging. *Biomaterials* **2016**, *101*, 121–30.
- (16) Wang, C.; Sun, X.; Cheng, L.; Yin, S.; Yang, G.; Li, Y.; Liu, Z. Multifunctional Theranostic Red Blood Cells for Magnetic-Field-Enhanced *In Vivo* Combination Therapy of Cancer. *Adv. Mater.* **2014**, *26*, 4794–802.
- (17) Ai, X.; Ho, C. J.; Aw, J.; Attia, A. B.; Mu, J.; Wang, Y.; Wang, X.; Wang, Y.; Liu, X.; Chen, H.; Gao, M.; Chen, X.; Yeow, E. K.; Liu, G.; Olivo, M.; Xing, B. *In vivo* Covalent Cross-Linking of Photon-Converted Rare-Earth Nanostructures for Tumour Localization and Theranostics. *Nat. Commun.* **2016**, *7*, 10432.
- (18) Lucky, S. S.; Idris, N. M.; Li, Z. Q.; Huang, K.; Soo, K. C.; Zhang, Y. Titania Coated Upconversion Nanoparticles for Near-Infrared Light Triggered Photodynamic Therapy. *ACS Nano* **2015**, *9*, 191–205.
- (19) Fan, W.; Bu, W.; Shi, J. On The Latest Three-Stage Development of Nanomedicines based on Upconversion Nanoparticles. *Adv. Mater.* **2016**, *28*, 3987–4011.
- (20) Zhou, J.; Liu, Z.; Li, F. Upconversion Nanophosphors for Small-Animal Imaging. *Chem. Soc. Rev.* **2012**, *41*, 1323–49.
- (21) Ni, D.; Bu, W.; Zhang, S.; Zheng, X.; Li, M.; Xing, H.; Xiao, Q.; Liu, Y.; Hua, Y.; Zhou, L.; Peng, W.; Zhao, K.; Shi, J. Single Ho³⁺-Doped Upconversion Nanoparticles for High-Performance T2-Weighted Brain Tumor Diagnosis and MR/UCL/CT Multimodal Imaging. *Adv. Funct. Mater.* **2014**, *24*, 6613–6620.
- (22) Xiao, Q.; Zheng, X.; Bu, W.; Ge, W.; Zhang, S.; Chen, F.; Xing, H.; Ren, Q.; Fan, W.; Zhao, K.; Hua, Y.; Shi, J. A Core/Satellite Multifunctional Nanotheranostic for *In Vivo* Imaging and Tumor Eradication by Radiation/Photothermal Synergistic Therapy. *J. Am. Chem. Soc.* **2013**, *135*, 13041–8.
- (23) Zhang, C.; Zhao, K.; Bu, W.; Ni, D.; Liu, Y.; Feng, J.; Shi, J. Marriage of Scintillator and Semiconductor for Synchronous Radiotherapy and Deep Photodynamic Therapy with Diminished Oxygen Dependence. *Angew. Chem., Int. Ed.* **2015**, *54*, 1770–4.
- (24) Lv, R.; Yang, P.; He, F.; Gai, S.; Yang, G.; Dai, Y.; Hou, Z.; Lin, J. An Imaging-Guided Platform for Synergistic Photodynamic/Photothermal/Chemo-Therapy with pH/Temperature-Responsive Drug Release. *Biomaterials* **2015**, *63*, 115–27.
- (25) Chen, B.; Dong, B.; Wang, J.; Zhang, S.; Xu, L.; Yu, W.; Song, H. Amphiphilic Silane Modified NaYF₄:Yb,Er Loaded with Eu(TTA)₃(TPPO)₂ Nanoparticles and Their Multi-functions: Dual Mode Temperature Sensing and Cell Imaging. *Nanoscale* **2013**, *5*, 8541–9.
- (26) Hu, F. Q.; Wei, L.; Zhou, Z.; Ran, Y. L.; Li, Z.; Gao, M. Y. Preparation of Biocompatible Magnetite Nanocrystals for *In Vivo* Magnetic Resonance Detection of Cancer. *Adv. Mater.* **2006**, *18*, 2553–2556.
- (27) Qian, H. S.; Guo, H. C.; Ho, P. C.; Mahendran, R.; Zhang, Y. Mesoporous-Silica-Coated Up-Conversion Fluorescent Nanoparticles for Photodynamic Therapy. *Small* **2009**, *5*, 2285–90.
- (28) Wang, X.; Liu, K.; Yang, G.; Cheng, L.; He, L.; Liu, Y.; Li, Y.; Guo, L.; Liu, Z. Near-Infrared Light Triggered Photodynamic Therapy in Combination with Gene Therapy Using Upconversion Nanoparticles for Effective Cancer Cell Killing. *Nanoscale* **2014**, *6*, 9198–205.
- (29) Zhang, C.; Yang, L.; Zhao, J.; Liu, B.; Han, M. Y.; Zhang, Z. White-Light Emission from an Integrated Upconversion Nanostructure: Toward Multicolor Displays Modulated by Laser Power. *Angew. Chem., Int. Ed.* **2015**, *54*, 11531–5.